frontiers | Frontiers in Chemistry

ORIGINAL RESEARCH
published: 30 June 2022
doi: 10.3389/fchem.2022.943902

# Electronic, Magnetic, and Optical Properties of Metal Adsorbed g-ZnO Systems

*Yang Shen[1]*, Zhihao Yuan[1], Zhen Cui[2]*, Deming Ma[1], Kunqi Yang[1], Yanbo Dong[1], Fangping Wang[1], Ai Du[3] and Enling Li[1]**

[1]School of Science, Xi'an University of Technology, Xi'an, China, [2]School of Automation and Information Engineering, Xi'an University of Technology, Xi'an, China, [3]Shanghai Key Laboratory of Special Artificial Microstructure Materials and Technology, School of Physics Science and Engineering, Tongji University, Shanghai, China

2D ZnO is one of the most attractive materials for potential applications in photocatalysis, gas and light detection, ultraviolet light-emitting diodes, resistive memory, and pressure-sensitive devices. The electronic structures, magnetic properties, and optical properties of M (Li, Na, Mg, Ca, or Ga) and TM (Cr, Co, Cu, Ag, or Au) adsorbed g-ZnO were investigated with density functional theory (DFT). It is found that the band structure, charge density difference, electron spin density, work function, and absorption spectrum of g-ZnO can be tuned by adsorbing M or TM atoms. More specifically, the specific charge transfer occurs between g-ZnO and adsorbed atom, indicating the formation of a covalent bond. The work functions of M adsorbed g-ZnO systems are obviously smaller than that of intrinsic g-ZnO, implying great potential in high-efficiency field emission devices. The Li, Na, Mg, Ca, Ga, Ag, or Au adsorbed g-ZnO systems, the Cr adsorbed g-ZnO system, and the Co or Cu adsorbed g-ZnO systems exhibit non-magnetic semiconductor proprieties, magnetic semiconductor proprieties, and magnetic metal proprieties, respectively. In addition, the magnetic moments of Cr, Co, or Cu adsorbed g-ZnO systems are 4 $\mu_B$, 3 $\mu_B$, or 1 $\mu_B$, respectively, which are mainly derived from adsorbed atoms, suggesting potential applications in nano-scale spintronics devices. Compared with the TM absorbed g-ZnO systems, the M adsorbed g-ZnO systems have more obvious absorption peaks for visible light, particularly for Mg or Ca adsorbed g-ZnO systems. Their absorption peaks appear in the near-infrared region, suggesting great potential in solar photocatalysis. Our work contributes to the design and fabrication of high-efficiency field emission devices, nano-scale spintronics devices, and visible-light responsive photocatalytic materials.

**Keywords: g-ZnO, magnetism, main group metal, transition metal, first-principles**

OPEN ACCESS

***Edited by:***
*Minglei Sun,*
*King Abdullah University of Science and Technology, Saudi Arabia*

***Reviewed by:***
*Xuming Wu,*
*Lingnan Normal University, China*
*Zhaoyong Guan,*
*Shandong University, China*

****Correspondence:***
*Yang Shen*
*448085355@qq.com*
*Zhen Cui*
*zcui@xaut.edu.cn*
*Enling Li*
*lienling@xaut.edu.cn*

***Specialty section:***
*This article was submitted to Theoretical and Computational Chemistry, a section of the journal Frontiers in Chemistry*

***Received:*** *14 May 2022*
***Accepted:*** *03 June 2022*
***Published:*** *30 June 2022*

***Citation:***
*Shen Y, Yuan Z, Cui Z, Ma D, Yang K, Dong Y, Wang F, Du A and Li E (2022) Electronic, Magnetic, and Optical Properties of Metal Adsorbed g-ZnO Systems. Front. Chem. 10:943902. doi: 10.3389/fchem.2022.943902*

## INTRODUCTION

The discovery of graphene (Novoselov et al., 2004) has stimulated research into other two-dimensional (2D) materials, such as transition metal dichalcogenides (TMDCs: $MoS_2$, $WSe_2$, $ReS_2$, $PtSe_2$, and $NbSe_2$), black and blue scales (Zhu and Tománek, 2014; Li et al., 2015; Zhao et al., 2017; Sun and Schwingenschlogl, 2020; Sun et al., 2021), silica, and transition metal oxides (TMOs) (Sahin et al., 2009; Sun and Schwingenschlögl, 2021a; Chen et al., 2021; Lv et al., 2021). Compared with three-dimensional (3D) bulk and wafer materials, 2D materials exhibit superior electron transport, optics, mechanics, and magnetic properties (Gong et al., 2017; Tan et al., 2017),

which have been applied in the fields of gas sensing (Zhang et al., 2010; Ziletti et al., 2015; Mahabal et al., 2016; Kooti et al., 2019; Sun et al., 2019), photocatalytic devices (Sun et al., 2017a; Wang et al., 2018a; Cui et al., 2020a), spintronic devices (Yuan et al., 2013; Sun et al., 2017b; Sun et al., 2018a; Cao et al., 2018) and piezoelectric devices (Komsa et al., 2012; Pospischil et al., 2014; Ross et al., 2014; He et al., 2015; Sun et al., 2017c; Sun et al., 2018b; Cui et al., 2020b; Cui et al., 2020c; Cui et al., 2021a; Cui et al., 2021b; Sun and Schwingenschlögl, 2021b).

As one of the II-VI direct bandgap semiconductor materials, ZnO exhibits the characteristics of a wide bandgap, strong radiation resistance, and high exciton binding energy, whose bandgap is about 3.37 eV and the exciton binding energy is up to 60 meV at room temperature (Tusche et al., 2007). ZnO exhibits piezoelectric effect, high chemical stability, high electrochemical coupling coefficient (Weirum et al., 2010), high activity, environmental friendliness, and low acquisition cost, therefore owning significant application potential in the fields of ultraviolet laser emitters, gas, and light detection (Pan et al., 2014; Sahoo et al., 2016; Zhang and Cui, 2022a), as well as photocatalysis (Guan et al., 2017; Guan et al., 2018).

Recently,Claeyssens et al. (2005) predicted the stable existence of graphene-like zinc oxide (g-ZnO). Zhang et al. (2014) report that B, N, or C doped g-ZnO exhibits strong chemisorption for CO. Wang et al. (Cui et al., 2019) conducted a mixed density functional study on the effects of rotation angle and biaxial strain on g-ZnO/TMDCs heterojunctions. In addition to doping and building heterojunctions, adsorption (Zhang and Cui, 2022b) is another efficient way to modify 2D materials. Cui et al. (Wang et al., 2018b; Cui et al., 2020d; Cui et al., 2021c) demonstrated the possibility of reducing the work function of g-GaN adsorption and increasing the absorption of visible light via absorbing transition metals (TMs). Guan et al. (2020) found that the adsorption of transition metal atoms onto graphene with extended-line defects induces magnetism and spin polarization. Wang et al. (2014) found that V, Cr, Fe, Co, Cu, Sc, or Mn absorbed $MoS_2$ showed magnetism. Chen et al. (2019) found that Cr, Mn, Fe, Co, or Cu absorbed g-GaN exhibited magnetism. Meanwhile, Zhao et al. (2013) successfully prepared graphene/ZnO composites and applied them to adsorb Cu (II), Pb (II) and Cr (III) in aqueous solution. Luo et al. (2017) synthesized g-ZnO nanosheets and used hybridization density functional theory to calculate cation-anion passivation co-doped g-ZnO for the design of efficient aqueous redox photocatalysts. According to our current knowledge, there are relatively few detailed reports on the adsorption of g-ZnO systems by M (Li, Na, Mg, Ca, or Ga) and TM (Cr, Co, Cu, Ag, or Au). The electronic structure, magnetic and optical properties of the g-ZnO after adsorption require more in-depth exploration.

Here, the electronic, magnetic, and optical properties of M (Li, Na, Mg, Ca, or Ga) and TM (Cr, Co, Cu, Ag, or Au) adsorbed g-ZnO systems were studied using the first-principles based on DFT. The band structure, charge density difference, electron spin density, work function, magnetic properties, and absorption spectrum of each system were analyzed, respectively. The results provide a theoretical basis for the design and fabrication of high-efficiency field emission devices, nano-scale spintronics devices, and visible-light responsive photocatalytic materials.

## CALCULATION METHODS AND MODELS

The electronic, magnetic and optical properties of M (Li, Na, Mg, Ca, or Ga) and TM (Cr, Co, Cu, Ag, or Au) adsorbed g-ZnO systems are calculated by adopting the first principles based on DFT. The electron exchange-correlation effects between electrons are treated using the generalized gradient approximation (GGA) in the Perdew-Burke-Ernzerhof (PBE) formula. Weak intermolecular dispersive forces are treated with Grimme's DFT-D3 method. The cutoff energy, the K point sampling in the Brillouin zone, the mechanical convergence standard, and the energy change of the atoms are set as 500 eV, 3 × 3 × 1, 0.01 eV $Å^{-1}$, and $10^{-5}$ eV, respectively. The model of g-ZnO is a 4 × 4 × 1 supercell, as displayed in **Figure 1A**.

Four different stable adsorption sites are named as $T_{Zn}$ (above the Zn atom), $T_O$ (above the O atom), $T_B$ (above the middle of the Zn-O bond), and $T_M$ (above the center of the hexagonal). The vacuum layer (20 Å in thickness) is added to reduce the interaction between periodic adjacent layers. All systems are geometrically optimized before calculating for obtaining the stable equilibrium state, which is judged by the adsorption energy ($E_{ad}$) calculated as follows:

$$E_{ad} = E_{total} - E_{g-ZnO} - \mu_{M/TM} \quad (1)$$

where $E_{ad}$ represents the adsorption energy, $E_{total}$, $E_{g\text{-}ZnO}$, and $\mu_{M/TM}$ are the total energy of M or TM adsorbed g-ZnO systems, intrinsic g-ZnO, and the chemical potential of adsorbed atoms, respectively. The Bader charge method is carried out for accurately calculating the charge transfer. The spin-polarized charge density ($\rho = \rho_{spin\text{-}up}\text{-}\rho_{spin\text{-}down}$) of the Cr, Co, or Cu adsorbed g-ZnO systems are calculated.

## RESULTS AND DISCUSSIONS

The energy band structure of intrinsic g-ZnO is shown in **Figure 1B**, which demonstrates that it is a direct semiconductor. The total density of state (TDOS) and the density of states for the contribution of electrons in different orbits are shown in **Figure 1C**. The adsorption energy ($E_{ad}$), charge transfer ($C$), magnetic moment ($M_{total}$), bandgap ($E_g$), and adsorption height ($D$) of the M or TM absorbed g-ZnO systems are listed in **Table 1**.

It is shown that the most stable adsorption sites and the adsorption heights of each system are both different. All systems are slightly deformed due to the interatomic interaction, as shown in **Figure 2**. Their charge differential densities (CDD) are calculated as follows:

$$\triangle\rho = \rho_{total} - \rho_{ZnO} - \rho_{M/TM} \quad (2)$$

where $\rho_{total}$, $\rho_{ZnO}$, and $\rho_{M/TM}$ presents the charge densities of M or TM adsorbed g-ZnO systems, intrinsic g-ZnO, and M or TM atoms,

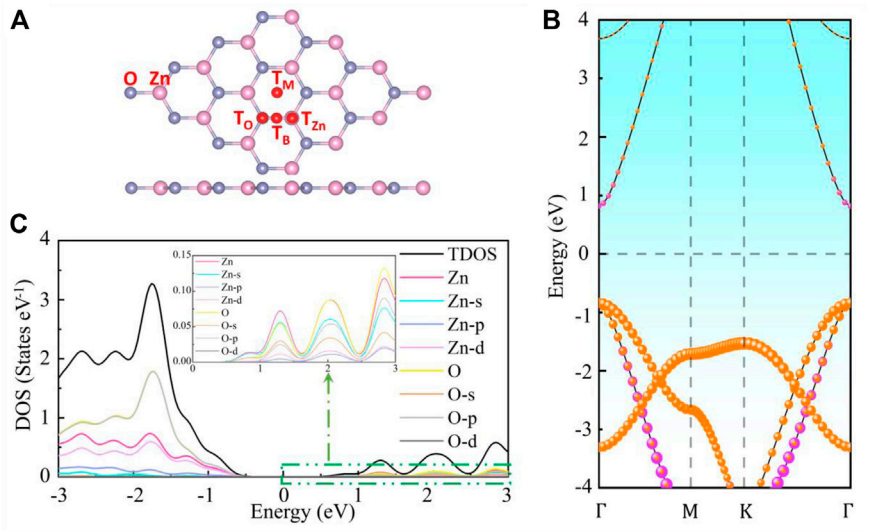


**FIGURE 1 |** The **(A)** crystal structure, **(B)** energy band structure, and **(C)** density of state of intrinsic g-ZnO.

**TABLE 1 |** The adsorption energy ($E_{ad}$), charge transfer ($C$), magnetic moment ($M_{total}$), bandgap ($E_g$), and adsorption height ($D$) of the M or TM absorbed g-ZnO systems.

| Type | Atom | Adsorption sites | $E_{ad}$ (eV) | $C$ (\|e\|) | $M_{total}$ ($\mu_B$) | $E_g$ (eV) | $D$ (Å) |
|---|---|---|---|---|---|---|---|
| M | Li | $T_M$ | −3.374 | −0.868 | 0 | 0 | 0.979 |
| | Na | $T_M$ | −2.283 | −0.814 | 0 | 0 | 1.559 |
| | Mg | $T_M$ | −2.975 | −1.340 | 0 | 0.613 | 1.065 |
| | Ca | $T_M$ | −5.971 | −1.478 | 0 | 0.908 | 1.259 |
| | Ga | $T_{Zn}$ | −4.203 | −0.680 | 0 | 0 | 1.433 |
| TM | Cr | $T_O$ | −3.161 | −0.360 | 4 | 2.068 | 1.865 |
| | Co | $T_M$ | −2.683 | −0.254 | 3 | 0.511 | 1.897 |
| | Cu | $T_M$ | −1.499 | −0.093 | 1 | 1.970 | 1.867 |
| | Ag | $T_M$ | −0.946 | −0.111 | 0 | 2.011 | 2.139 |
| | Au | $T_O$ | −1.395 | +0.127 | 0 | 1.982 | 2.019 |

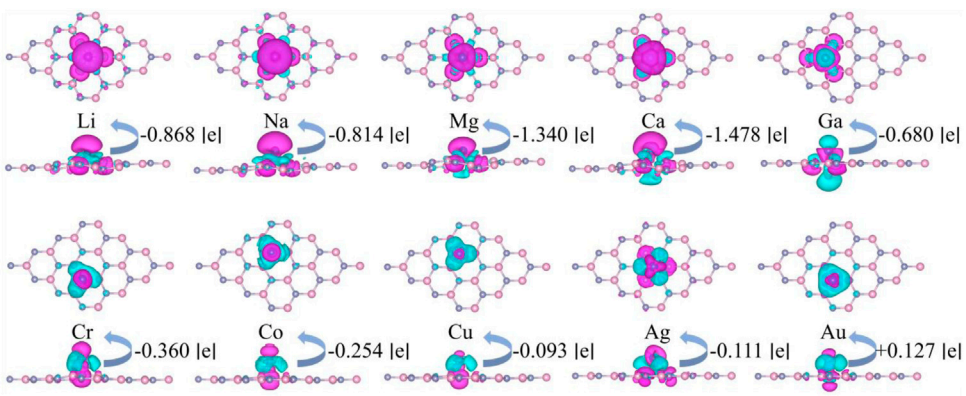


**FIGURE 2 |** The differential charge density of M or TM adsorbed g-ZnO systems. The blue area and purple area represent electron aggregation and electron dissipation, respectively. And the iso-value is set as $5 \times 10^{-4}$ e Å$^{-3}$.

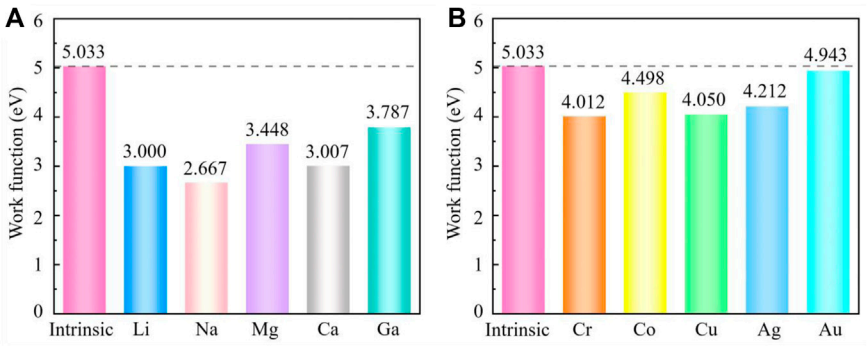


**FIGURE 3 |** The work functions of the intrinsic g-ZnO and **(A)** M or **(B)** TM adsorbed g-ZnO systems.

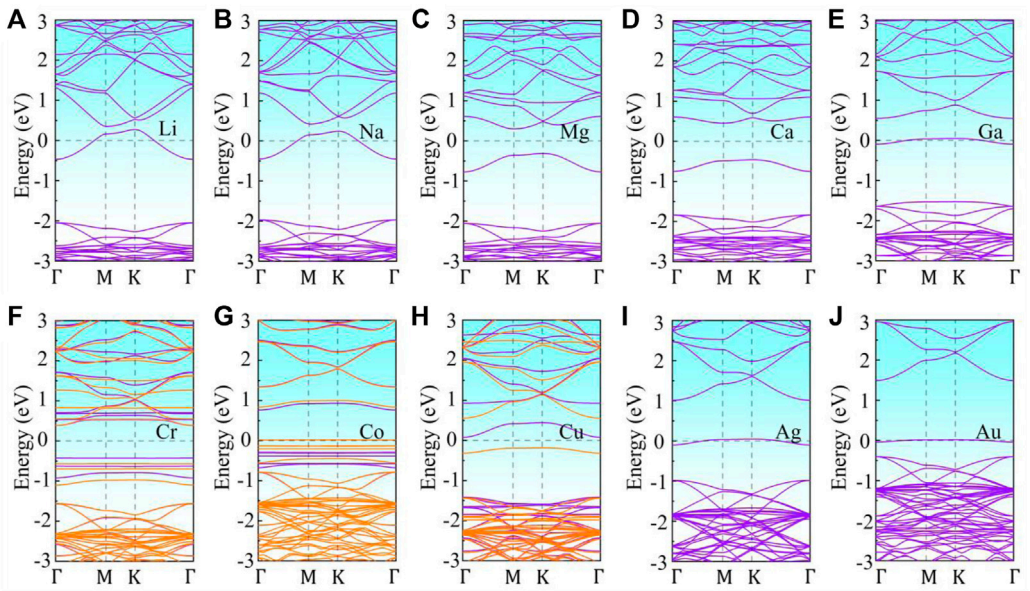


**FIGURE 4 |** The band structures of M or TM adsorbed g-ZnO systems: **(A)** Li, **(B)** Na, **(C)** Mg, **(D)** Ca, **(E)** Ga, **(F)** Cr, **(G)** Co, **(H)** Cu, **(I)** Ag, **(J)** Au. Purple line indicates spin up, and orange line denotes spin down. The Fermi level is shifted to zero.

respectively. The differential charge density of M or TM adsorbed g-ZnO systems are illustrated in **Figure 2**, where the specific charge transfer occurred between ZnO and M or TM, which indicates the formation of a covalent bond between ZnO and M or TM atoms.

The redistribution of charge leads to the creation of a dipole moment, which causes a change in the work function. The work functions are shown in **Figure 3**. Especially, Na adsorbed g-ZnO system has the lowest work function of 2.667 eV, about 47% lower than that of intrinsic g-ZnO. All adsorption systems have lower work functions than the intrinsic g-ZnO. At the same time, M adsorbed g-ZnO systems have much lower work functions than those of TM adsorbed g-ZnO systems, indicating that M adsorbed g-ZnO systems have strong field emission capabilities.

To further investigate the effect of metal adsorption on the electronic properties and magnetic properties of monolayer g-ZnO, the energy band structure of the adsorbed system was calculated. The band structure of M or TM adsorbed g-ZnO systems are shown in **Figure 4**. The gap of the Ca, Mg, Ni, or Pt adsorbed g-ZnO systems are 0.908 eV, 0.613 eV, 2.497 eV, or 2.560 eV, respectively, exhibiting characteristics of non-magnetic semiconductors. The gap of Cr adsorbed g-ZnO system is 2.068 eV, exhibiting characteristics of a magnetic semiconductor. The gap of the Co or Cu adsorbed g-ZnO systems are 0.511 eV or 1.970 eV, respectively, exhibiting characteristics of magnetic metals.

For further investigating the derivation mechanism of magnetism, the spin-polarized charge density ($\rho = \rho_{\text{spin-up}}$-$\rho_{\text{spin-down}}$) of the Cr, Co, or Cu adsorbed g-ZnO systems are calculated, as shown in **Figure 5**. The magnetic moments of the Cr, Co, or Cu adsorbed g-ZnO systems are 4 $\mu_B$, 3 $\mu_B$, or 1 $\mu_B$, respectively. Cui et al. reported that the Co and Cu adsorbed $Pb_2Se_3$ systems produced

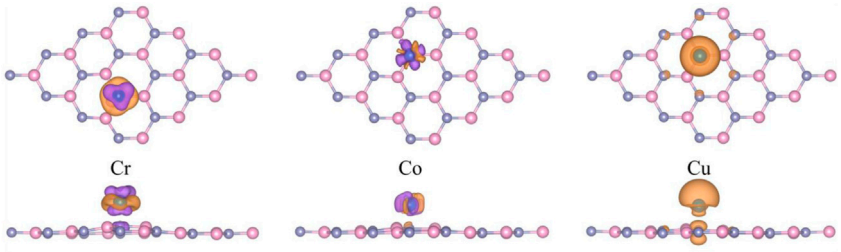


**FIGURE 5 |** The spin-polarized charge density of Cr, Co, or Cu adsorbed g-ZnO systems. The purple areas represent spin up, and the orange areas represent spin down. And the iso-value is $1 \times 10^{-3}$ e Å$^{-3}$.

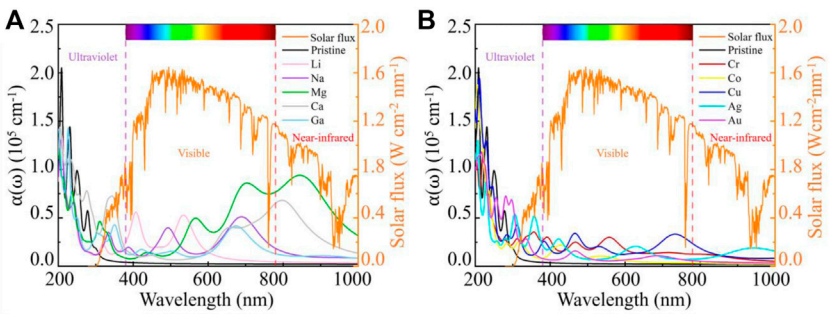


**FIGURE 6 |** Absorption spectrum of intrinsic g-ZnO and **(A)** M or **(B)** TM adsorbed g-ZnO systems.

magnetic moments of 0.152 $\mu_B$ and 0.491 $\mu_B$, respectively (Cui et al., 2022). Our results are similar to theirs. From **Figure 5**, it can be observed that the magnetic moments are mainly derived from adsorbed transition metal atoms. The results suggest the possibility of tuning the magnetic properties of g-ZnO by adsorbing Cr, Co, or Cu as well the potential of applications in nano-scale spintronics devices.

The light absorption coefficients [$\alpha(\omega)$] of intrinsic g-ZnO and M or TM adsorbed g-ZnO systems are calculated as follows:

$$\alpha(\omega) = \sqrt{2\omega}\left[\sqrt{\varepsilon_1^2(\omega) + \varepsilon_2^2(\omega)} - \varepsilon_1(\omega)\right]^{\frac{1}{2}} \quad (3)$$

where $\omega$, $\varepsilon_1(\omega)$, and $\varepsilon_2(\omega)$ are the frequency of the photon, real part, and imaginary part of the dielectric constant, respectively. The absorption spectrum of the intrinsic ZnO and metal adsorbed g-ZnO systems are shown in **Figure 6**. It is shown that the intrinsic g-ZnO has almost no absorption of visible light, while M or TM adsorbed g-ZnO systems have several firm absorption peaks in the visible light region. For example, the absorption peaks of the Li, Na, or Mg adsorbed g-ZnO system are located at 406.6 nm and 534.2 nm, 492.4 nm and 689.2 nm, or 567.6 nm and 704.8 nm, respectively. In addition, the absorption peaks of the Cu adsorbed g-ZnO system are located at 465.1 nm and 733.7 nm. In particular, the $\alpha(\omega)$ of the Mg adsorbed g-ZnO system is up to $8.633 \times 10^4$ cm$^{-1}$ at 704.8 nm. At the same time, Cui et al. (2018) reported the optical properties of g-GaN adsorbed by alkali metals with an absorption peak in the range of 551 nm–708 nm with an absorption coefficient of $2.5 \times 10^4$ cm$^{-1}$. Ren et al. (2019) reported a two-dimensional van der Waals heterostructure based on ZnO/Mg(OH)$_2$ with an absorption peak of $4.8 \times 10^4$ cm$^{-1}$ at 415.75 nm. Xia et al. (2022) reported a two-dimensional GaN/ZnO heterostructure with an absorption peak in the visible range with an intensity of about $2 \times 10^4$ cm$^{-1}$. The reports of the above scholars are similar to our results. This indicated significant potential value in visible-light photocatalytic. In addition, the Mg or Ca adsorbed g-ZnO systems have prominent absorption peaks for the near-infrared region, also meaning the potential in solar photocatalysis. Therefore, the optical properties of g-ZnO can be effectively tuned by adsorbing Li, Na, Mg, Ca, or Cu.

In general, compared with the TM absorbed g-ZnO systems, the M adsorbed g-ZnO systems have more obvious absorption peaks for visible light, particularly for Mg or Ca adsorbed g-ZnO systems. Their absorption peaks appear in the near-infrared region, suggesting great potential in solar photocatalysis.

## CONCLUSION

The electronic, magnetic and optical properties of M (Li, Na, Mg, Ca, or Ga) and TM (Cr, Co, Cu, Ag, or Au) adsorbed g-ZnO systems were studied using the first-principles on DFT. It is found that the band structure, charge density difference, electron spin density, work function, and absorption spectrum of g-ZnO can be tuned by adsorbing M or TM atoms. The work functions of M adsorbed g-ZnO systems are obviously smaller than that of intrinsic g-ZnO, implying great potential in high-efficiency field emission devices.

The Li, Na, Mg, Ca, Ga, Ag, or Au adsorbed g-ZnO systems, the Cr adsorbed g-ZnO system, and the Co or Cu adsorbed g-ZnO systems exhibit non-magnetic semiconductor proprieties, magnetic semiconductor proprieties, and magnetic metal proprieties, respectively. In addition, the magnetic moments of Cr, Co, or Cu adsorbed g-ZnO systems are 4 $\mu_B$, 3 $\mu_B$, or 1 $\mu_B$, respectively, which are mainly derived from adsorbed atoms, suggesting potential applications in nano-scale spintronics devices. Compared with the TM absorbed g-ZnO systems, the M adsorbed g-ZnO systems have more obvious absorption peaks for visible light, particularly for Mg or Ca adsorbed g-ZnO systems. Their absorption peaks appear in the near-infrared region, suggesting great potential in solar photocatalysis. Our work contributes to the design and fabrication of high-efficiency field emission devices, nano-scale spintronics devices, and visible-light responsive photocatalytic materials.

## DATA AVAILABILITY STATEMENT

The raw data supporting the conclusions of this article will be made available by the authors, without undue reservation.

## AUTHOR CONTRIBUTIONS

YS, ZC, and EL contributed to conception and design of the study. ZY organized the database. DM performed the statistical analysis. YS and ZY wrote the first draft of the manuscript. KY, YD, FW, and AD wrote sections of the manuscript. All authors contributed to manuscript revision, read, and approved the submitted version.

## FUNDING

This work was funded by Natural Science Basic Research Program of Shaanxi (Program No. 2022JM-176), Scientific Research Program Funded by Shaanxi Provincial Education Department (Program No. 21JK0789), the Opening Project of Shanghai Key Laboratory of Special Artificial Microstructure Materials and Technology (Program No. ammt2020A-6), College Students' Innovative Entrepreneurial Training Plan Program (Program No. G202110700010 and Program No. X202110700213), the National Natural Science Foundation of China (No. 12104362) and China Postdoctoral Science Foundation (Program No. 2020M683684XB).

## REFERENCES

Cao, Y., Fatemi, V., Fang, S., Watanabe, K., Taniguchi, T., Kaxiras, E., et al. (2018). Unconventional Superconductivity in Magic-Angle Graphene Superlattices. *Nature* 556, 43–50. doi:10.1038/nature26160

Chen, G.-X., Li, H.-F., Wang, D.-D., Li, S.-Q., Fan, X.-B., and Zhang, J.-M. (2019). Adsorption of Toxic Gas Molecules on Pristine and Transition Metal Doped Hexagonal GaN Monolayer: A First-Principles Study. *Vacuum* 165, 35–45. doi:10.1016/j.vacuum.2019.04.001

Chen, Z.-L., Wang, D., Wang, X.-Y., and Yang, J.-H. (2021). Enhanced Formaldehyde Sensitivity of Two-Dimensional Mesoporous SnO2 by Nitrogen-Doped Graphene Quantum Dots. *Rare Mater.* 40, 1561–1570. doi:10.1007/s12598-020-01636-6

Claeyssens, F., Freeman, C. L., Allan, N. L., Sun, Y., Ashfold, M. N. R., and Harding, J. H. (2005). Growth of ZnO Thin Films-Experiment and Theory. *J. Mat. Chem.* 15, 139–148. doi:10.1039/b414111c

Cui, Z., Bai, K., Ding, Y., Wang, X., Li, E., and Zheng, J. (2020). Janus XSSe/SiC (X = Mo, W) van der Waals heterostructures as promising water-splitting photocatalysts. *Phys. E Low-dimensional Syst. Nanostructures* 123, 114207. doi:10.1016/j.physe.2020.114207

Cui, Z., Bai, K., Ding, Y., Wang, X., Li, E., Zheng, J., et al. (2020). Electronic and Optical Properties of Janus MoSSe and ZnO vdWs Heterostructures. *Superlattices Microstruct.* 140, 106445. doi:10.1016/j.spmi.2020.106445

Cui, Z., Bai, K., Wang, X., Li, E., and Zheng, J. (2020). Electronic, Magnetism, and Optical Properties of Transition Metals Adsorbed G-GaN. *Phys. E Low-dimensional Syst. Nanostructures* 118, 113871. doi:10.1016/j.physe.2019.113871

Cui, Z., Luo, Y., Yu, J., and Xu, Y. (2021). Tuning the Electronic Properties of MoSi2N4 by Molecular Doping: A First Principles Investigation. *Phys. E Low-dimensional Syst. Nanostructures* 134, 114873. doi:10.1016/j.physe.2021.114873

Cui, Z., Lyu, N., Ding, Y., Bai, K., Ding, Y., and Bai, K. (2021). Noncovalently Functionalization of Janus MoSSe Monolayer with Organic Molecules. *Phys. E Low-dimensional Syst. Nanostructures* 127, 114503. doi:10.1016/j.physe.2020.114503

Cui, Z., Ren, K., Zhao, Y., Wang, X., Shu, H., Yu, J., et al. (2019). Electronic and optical properties of van der Waals heterostructures of g-GaN and transition metal dichalcogenides. *Appl. Surf. Sci.* 492, 513–519. doi:10.1016/j.apsusc.2019.06.207

Cui, Z., Wang, M., Lyu, N., Zhang, S., Ding, Y., and Bai, K. (2021). Electronic, Magnetism and Optical Properties of Transition Metals Adsorbed Puckered Arsenene. *Superlattices Microstruct.* 152, 106852. doi:10.1016/j.spmi.2021.106852

Cui, Z., Wang, X., Ding, Y., Li, E., Bai, K., Zheng, J., et al. (2020). Adsorption of CO, NH3, NO, and NO2 on Pristine and Defective g-GaN: Improved Gas Sensing and Functionalization. *Appl. Surf. Sci.* 530, 147275. doi:10.1016/j.apsusc.2020.147275

Cui, Z., Wang, X., Li, E., Ding, Y., Sun, C., and Sun, M. (2018). Alkali-metal-adsorbed G-GaN Monolayer: Ultralow Work Functions and Optical Properties. *Nanoscale Res. Lett.* 13, 207. doi:10.1186/s11671-018-2625-z

Cui, Z., Zhang, S., Wang, L., and Yang, K. (2022). Optoelectronic and Magnetic Properties of Transition Metals Adsorbed Pd2Se3 Monolayer. *Micro Nanostructures* 167, 207260. doi:10.1016/j.micrna.2022.207260

Gong, C., Li, L., Li, Z., Ji, H., Stern, A., Xia, Y., et al. (2017). Discovery of intrinsic ferromagnetism in two-dimensional van der Waals crystals. *Nature* 546, 265–269. doi:10.1038/nature22060

Guan, Z., Lian, C.-S., Hu, S., Ni, S., Li, J., and Duan, W. (2017). Tunable Structural, Electronic, and Optical Properties of Layered Two-Dimensional C2N and MoS2 van der Waals Heterostructure as Photovoltaic Material. *J. Phys. Chem. C* 121, 3654–3660. doi:10.1021/acs.jpcc.6b12681

Guan, Z., Ni, S., and Hu, S. (2020). First-Principles Study of 3d Transition-Metal-Atom Adsorption onto Graphene Embedded with the Extended Line Defect. *ACS Omega* 5, 5900–5910. doi:10.1021/acsomega.9b04154

Guan, Z., Ni, S., and Hu, S. (2018). Tunable Electronic and Optical Properties of Monolayer and Multilayer Janus MoSSe as a Photocatalyst for Solar Water Splitting: A First-Principles Study. *J. Phys. Chem. C* 122, 6209–6216. doi:10.1021/acs.jpcc.8b00257

He, Y.-M., Clark, G., Schaibley, J. R., He, Y., Chen, M.-C., Wei, Y.-J., et al. (2015). Single Quantum Emitters in Monolayer Semiconductors. *Nat. Nanotech* 10, 497–502. doi:10.1038/nnano.2015.75

Komsa, H., Kotakoski, J., Kurasch, S., Lehtinen, O., Kaise, U., and Krasheninnikov, A. (2012). TWo-Dimensional Transition Metal Dichalcogenides under Electron Irradiation: Defect Production and Doping. *Phys. Rev. Lett.* 109, 035503. doi:10.1103/physrevlett.109.035503

Kooti, M., Keshtkar, S., Askarieh, M., and Rashidi, A. (2019). Progress toward a Novel Methane Gas Sensor Based on SnO2 Nanorods-Nanoporous Graphene Hybrid. *Sensors Actuators B Chem.* 281, 96–106. doi:10.1016/j.snb.2018.10.032

Li, Q.-F., Duan, C.-G., Wan, X. G., and Kuo, J.-L. (2015). Theoretical Prediction of Anode Materials in Li-Ion Batteries on Layered Black and Blue Phosphorus. *J. Phys. Chem. C* 119, 8662–8670. doi:10.1021/jp512411g

Luo, X., Wang, G., Huang, Y., Wang, B., Yuan, H., and Chen, H. (2017). Bandgap Engineering of the G-ZnO Nanosheet via Cationic-Anionic Passivated Codoping for Visible-Light-Driven Photocatalysis. *J. Phys. Chem. C* 121, 18534–18543. doi:10.1021/acs.jpcc.7b03616

Lv, H., Wu, C., Tang, J., Du, H., Qin, F., Peng, H., et al. (2021). Two-dimensional SnO/SnO2 Heterojunctions for Electromagnetic Wave Absorption. *Chem. Eng. J.* 411, 128445. doi:10.1016/j.cej.2021.128445

Mahabal, M. S., Deshpande, M. D., Hussain, T., and Ahuja, R. (2016). Sensing Characteristics of Phosphorene Monolayers toward PH3 and AsH3 Gases upon the Introduction of Vacancy Defects. *J. Phys. Chem. C* 120, 20428–20436. doi:10.1021/acs.jpcc.6b06791

Novoselov, K. S., Geim, A. K., Morozov, S. V., Jiang, D., Zhang, Y., Dubonos, S. V., et al. (2004). Electric Field Effect in Atomically Thin Carbon Films. *Science* 306, 666–669. doi:10.1126/science.1102896

Pan, Q., Liu, B. H., McBriarty, M. E., Martynova, Y., Groot, I. M. N., Wang, S., et al. (2014). Reactivity of Ultra-thin ZnO Films Supported by Ag(111) and Cu(111): A Comparison to ZnO/Pt(111). *Catal. Lett.* 144, 648–655. doi:10.1007/s10562-014-1191-y

Pospischil, A., Furchi, M. M., and Mueller, T. (2014). Solar-energy Conversion and Light Emission in an Atomic Monolayer P-N Diode. *Nat. Nanotech* 9, 257–261. doi:10.1038/nnano.2014.14

Ren, K., Yu, J., and Tang, W. (2019). First-principles study of two-dimensional van der Waals heterostructure based on ZnO and Mg(OH)2: A potential photocatalyst for water splitting. *Phys. Lett. A* 383, 125916. doi:10.1016/j.physleta.2019.125916

Ross, J. S., Klement, P., Jones, A. M., Ghimire, N. J., Yan, J., Mandrus, D. G., et al. (2014). Electrically Tunable Excitonic Light-Emitting Diodes Based on Monolayer WSe2 P-N Junctions. *Nat. Nanotech* 9, 268–272. doi:10.1038/nnano.2014.26

Sahin, H., Cahangirov, S., Topsakal, M., Bekaroglu, E., Akturk, E., Senger, R. T., et al. (2009). Monolayer Honeycomb Structures of Group-IV Elements and III-V Binary Compounds: First-Principles Calculation. *Phys. Rev. B* 80, 155453. doi:10.1103/PhysRevB.80.155453

Sahoo, T., Nayak, S. K., Chelliah, P., Rath, M. K., and Parida, B. (2016). Observations of Two-Dimensional Monolayer Zinc Oxide. *Mater. Res. Bull.* 75, 134–138. doi:10.1016/j.materresbull.2015.11.043

Sun, M., Chou, J.-P., Gao, J., Cheng, Y., Hu, A., Tang, W., et al. (2018). Exceptional Optical Absorption of Buckled Arsenene Covering a Broad Spectral Range by Molecular Doping. *ACS Omega* 3, 8514–8520. doi:10.1021/acsomega.8b01192

Sun, M., Chou, J.-P., Ren, Q., Zhao, Y., Yu, J., and Tang, W. (2017). Tunable Schottky barrier in van der Waals heterostructures of graphene and g-GaN. *Appl. Phys. Lett.* 110, 173105. doi:10.1063/1.4982690

Sun, M., Chou, J.-P., Shi, L., Gao, J., Hu, A., Tang, W., et al. (2018). Few-Layer PdSe2 Sheets: Promising Thermoelectric Materials Driven by High Valley Convergence. *ACS Omega* 3, 5971–5979. doi:10.1021/acsomega.8b00485

Sun, M., Chou, J.-P., Yu, J., and Tang, W. (2017). Effects of Structural Imperfection on the Electronic Properties of graphene/WSe2 Heterostructures. *J. Mat. Chem. C* 5, 10383–10390. doi:10.1039/c7tc03131a

Sun, M., Chou, J.-P., Yu, J., and Tang, W. (2017). Electronic Properties of Blue Phosphorene/graphene and Blue Phosphorene/graphene-like Gallium Nitride Heterostructures. *Phys. Chem. Chem. Phys.* 19, 17324–17330. doi:10.1039/c7cp01852e

Sun, M., Luo, Y., Yan, Y., and Schwingenschlogl, U. (2021). Ultrahigh Carrier Mobility in the Two-Dimensional Semiconductors B8Si4, B8Ge4, and B8Sn4. *Chem. Mat.* 33, 6475–6483. doi:10.1021/acs.chemmater.1c01824

Sun, M., and Schwingenschlogl, U. (2020). δ-CS: A Direct-Band-Gap Semiconductor Combining Auxeticity, Ferroelasticity, and Potential for High-Efficiency Solar Cells. *Phys. Rev. Appl.* 14, 044015. doi:10.1103/PhysRevApplied.14.044015

Sun, M., and Schwingenschlögl, U. (2021). Structure Prototype Outperforming MXenes in Stability and Performance in Metal-Ion Batteries: A High Throughput Study. *Adv. Energy Mat.* 11, 2003633. doi:10.1002/aenm.202003633

Sun, M., and Schwingenschlögl, U. (2021). Unique Omnidirectional Negative Poisson's Ratio in δ-Phase Carbon Monochalcogenides. *J. Phys. Chem. C* 125, 4133–4138. doi:10.1021/acs.jpcc.0c11555

Sun, S., Hussain, T., Zhang, W., and Karton, A. (2019). Blue Phosphorene Monolayers as Potential Nano Sensors for Volatile Organic Compounds under Point Defects. *Appl. Surf. Sci.* 486, 52–57. doi:10.1016/j.apsusc.2019.04.223

Tan, C., Cao, X., Wu, X.-J., He, Q., Yang, J., Zhang, X., et al. (2017). Recent Advances in Ultrathin Two-Dimensional Nanomaterials. *Chem. Rev.* 117, 6225–6331. doi:10.1021/acs.chemrev.6b00558

Tusche, C., Meyerheim, H. L., and Kirschner, J. (2007). Observation of Depolarized ZnO(0001) Monolayers: Formation of Unreconstructed Planar Sheets. *Phys. Rev. Lett.* 99, 026102. doi:10.1103/physrevlett.99.026102

Wang, G., Li, D., Sun, Q., Dang, S., Zhong, M., Xiao, S., et al. (2018). Hybrid Density Functional Study on the Photocatalytic Properties of Two-Dimensional G-ZnO Based Heterostructures. *Nanomaterials* 8, 374. doi:10.3390/nano8060374

Wang, S., Ren, C., Tian, H., Yu, J., and Sun, M. (2018). MoS2/ZnO van der Waals heterostructure as a high-efficiency water splitting photocatalyst: a first-principles study. *Phys. Chem. Chem. Phys.* 20, 13394–13399. doi:10.1039/c8cp00808f

Wang, Y., Wang, B., Huang, R., Gao, B., Kong, F., and Zhang, Q. (2014). First-principles Study of Transition-Metal Atoms Adsorption on MoS2 Monolayer. *Phys. E Low-dimensional Syst. Nanostructures* 63, 276–282. doi:10.1016/j.physe.2014.06.017

Weirum, G., Barcaro, G., Fortunelli, A., Weber, F., Schennach, R., Surnev, S., et al. (2010). Growth and Surface Structure of Zinc Oxide Layers on a Pd(111) Surface. *J. Phys. Chem. C* 114, 15432–15439. doi:10.1021/jp104620n

Xia, S., Diao, Y., and Kan, C. (2022). Electronic and Optical Properties of Two-Dimensional GaN/ZnO Heterojunction Tuned by Different Stacking Configurations. *J. Colloid Interface Sci.* 607, 913–921. doi:10.1016/j.jcis.2021.09.050

Yuan, H., Bahramy, M. S., Morimoto, K., Wu, S., Nomura, K., Yang, B.-J., et al. (2013). Zeeman-type Spin Splitting Controlled by an Electric Field. *Nat. Phys.* 9, 563–569. doi:10.1038/nphys2691

Zhang, L., and Cui, Z. (2022). Electronic, Magnetic, and Optical Performances of Non-metals Doped Silicon Carbide. *Front. Chem.* 10, 898174. doi:10.3389/fchem.2022.898174

Zhang, L., and Cui, Z. (2022). Theoretical Study on Electronic, Magnetic and Optical Properties of Non-metal Atoms Adsorbed onto Germanium Carbide. *Nanomaterials* 12, 1712. doi:10.3390/nano12101712

Zhang, Y.-H., Zhang, M.-L., Zhou, Y.-C., Zhao, J.-H., Fang, S.-M., and Li, F. (2014). Tunable Electronic and Magnetic Properties of Graphene-like ZnO Monolayer upon Doping and CO Adsorption: a First-Principles Study. *J. Mat. Chem. A* 2, 13129–13135. doi:10.1039/c4ta01874e

Zhang, Y., Tang, Z.-R., Fu, X., and Xu, Y.-J. (2010). TiO2–Graphene Nanocomposites for Gas-Phase Photocatalytic Degradation of Volatile Aromatic Pollutant: Is TiO2–Graphene Truly Different from Other TiO2–Carbon Composite Materials? *ACS Nano* 4, 7303–7314. doi:10.1021/nn1024219

Zhao, X., Hu, B., Ye, J., and Jia, Q. (2013). Preparation, Characterization, and Application of Graphene-Zinc Oxide Composites (G-ZnO) for the Adsorption of Cu(II), Pb(II), and Cr(III). *J. Chem. Eng. Data* 58, 2395–2401. doi:10.1021/je400384z

Zhao, Y., Tong, L., Li, Z., Yang, N., Fu, H., Wu, L., et al. (2017). Stable and Multifunctional Dye-Modified Black Phosphorus Nanosheets for Near-Infrared Imaging-Guided Photothermal Therapy. *Chem. Mat.* 29, 7131–7139. doi:10.1021/acs.chemmater.7b01106

Zhu, Z., and Tománek, D. (2014). Semiconducting Layered Blue Phosphorus: A Computational Study. *Phys. Rev. Lett.* 112, 176802. doi:10.1103/physrevlett.112.176802

Ziletti, A., Carvalho, A., Campbell, D. K., Coker, D. F., and Neto, A. H. C. (2015). Oxygen Defects in Phosphorene. *Phys. Rev. Lett.* 114, 046801. doi:10.1103/physrevlett.114.046801

**Conflict of Interest:** The authors declare that the research was conducted in the absence of any commercial or financial relationships that could be construed as a potential conflict of interest.